Research Article | Vol. 31, No. 15 / 17 Jul 2023 / Optics Express 24203
Optics EXPRESS

Electro-optical tunable interleaver in hybrid silicon and lithium niobate thin films

QINGYUN LI, HOUBIN ZHU, HONGHU ZHANG, AND HUI HU*

School of Physics, Shandong University, No. 27 South Shanda Road, Jinan 250100, China
**hhu@sdu.edu.cn*

Abstract: The interleaver was one of the key devices in dense wavelength division multiplexing (DWDM) applications. In this study, an interleaver with an asymmetrical Mach-Zehnder interferometer structure was designed, fabricated, and characterized in hybrid silicon and lithium niobate thin films (Si-LNOI). The interleaver based on Si-LNOI could be fabricated by mature processing technology of Si photonic, and it was capable of the electro-optical (E-O) tuning function by using the E-O effect of LN. In the range of 1530–1620 nm, the interleaver achieved a channel spacing of 55 GHz and an extinction ratio of 12–28 dB. Due to the large refractive index of Si, the Si loading strip waveguide based on Si-LNOI had a compact optical mode area, which allowed a small electrode gap to improve the E-O modulation efficiency of the interleaver. For an E-O interaction length of 1 mm, the E-O modulation efficiency was 26 pm/V. The interleaver will have potential applications in DWDM systems, optical switches, and filters.

1. Introduction

Due to the increasing amount of information exchange, wavelength division multiplexing (WDM) technology development has trended towards denser wavelength division multiplexing (DWDM) technology with narrower spacing. An interleaver can divide a group of densely spaced wavelengths into two groups of sparsely spaced and interleaved wavelengths, or combine two groups of sparsely spaced and interleaved wavelengths into one group of densely spaced wavelengths, which could meet the requirements of DWDM for a narrow channel and was widely used [1,2]. In the field of optical communication, the operating wavelength of the interleaver need to operate at a specific wavelength. However, the operating wavelength is easily affected by fabrication error and the external environment (such as humidity or temperature), resulting in the drift of the operating wavelength. Therefore, operating wavelength tunability of the interleaver is necessary for practical applications.

Waveguide-based interleavers can achieve electrical tuning in Si photonic circuits using the thermo-optical (T-O) effect [3,4]. However, the T-O effect suffers from slow response and high energy consumption, thus motivating alternative solutions based on materials with a strong electro-optical (E-O) effect. LNOI (lithium niobate on insulator) was identified as a promising integrated optical material platform with an excellent E-O effect, which could achieve a fast response and a low energy consumption [5–7]. A 1×2 reconfigurable E-O tunable interleaver in LNOI achieved channel spacing of 49.7 GHz. The length and gap of the electrodes were 1.35 mm and 3.5 µm, respectively. The wavelength tuning sensitivity of TE and TM modes is approximately 18 and 16 pm/V, respectively. The extinction ratios (ER) were 10–20 and 12–23 dB for TE and TM modes, respectively [8]. A 1×4 reconfigurable E-O tunable interleaver in LNOI (the length and gap of the electrodes were 3.9 mm and 5 µm, respectively) achieved switching voltages of 4.5 V and 6.7 V, and ER of 8–15 dB and 7–13 dB for TE and TM modes, respectively [9].

Hybrid mono-crystalline silicon and lithium niobate thin films (Si-LNOI) combines the remarkable electrical properties and mature micro-nano processing technology of Si, as well as the excellent optical properties of LN. The Si-LNOI therefore provides a new material platform for

#494532 https://doi.org/10.1364/OE.494532
Journal © 2023 Received 1 May 2023; revised 26 Jun 2023; accepted 27 Jun 2023; published 7 Jul 2023

Optics EXPRESS

integrated photonics [10]. Various photonic devices have been proposed and achieved in Si-LNOI, such as E-O modulators [11,12], spot-size converters (SSC) [13], and nonlinear conversion devices [14]. Due to the large refractive index of Si, the Si loading strip waveguide based on Si-LNOI had a compact optical mode area, which allowed a small electrode gap to enhance the overlap of the optical field and the electrostatic field. Therefore, E-O devices based on Si-LNOI could achieve high modulation efficiency and compact structure dimension [11].

In this study, an E-O tunable interleaver with an asymmetrical Mach-Zehnder interferometer (AMZI) structure was demonstrated in Si-LNOI. The AMZI structure was fabricated by forming Si waveguides using plasma etching, and it consisted of two 3 dB multimode interference (MMI) couplers and asymmetric arms between the MMIs. The simulation results showed that the insertion losses (ILs) for 1×2 and 2×2 MMIs were 0.055 and 0.117 dB, respectively, with large fabrication tolerances and small volume. At 1530–1620 nm, the interleaver achieved channel spacing of 55 GHz and ER of 12–28 dB. The interleaver had an electrically tunable sensitivity of 26 pm/V for a 1 mm E-O interaction length.

2. Design and simulation

The Si-LNOI could be fabricated by bonding Si thin film on LNOI. In the simulation, the LN thin film was X-cut with a thickness of 500 nm. The thicknesses of the SiO_2 layer and Si substrate were 2 and 500 μm, respectively. There was a trade-off between the optical power in the LN layer and the optical mode area (compact mode areas allowing a small electrode gap) [11]. The thickness of the Si thin film was designed to be 100 nm. Figure 1(a) shows a schematic of the E-O tunable interleaver in Si-LNOI. From top to bottom, the structure consists of AMZI structure and metal electrodes, LN thin film, SiO_2 layer, and Si substrate. Figure 1(b) shows a top view of the E-O tunable interleaver. The interleaver consisted of two 3 dB MMIs and asymmetric arms between the MMIs. Eight 90° circular bends were used to connect the MMIs and the straight waveguides. The widths of the straight and curved waveguides were designed to be 800 nm to operate in single mode condition. Figure 2(a) and (b) show the simulated optical TE modes of the Si loading strip waveguide and LNOI waveguide (at 1550 nm), respectively. It was simulated by the full-vectorial finite-difference method using MODE within Lumerical's DEVICE Multiphysics Simulation Suite (Ansys Canada Ltd., Canada). For the Si loading strip waveguide, the optical mode area was only 0.34 μm^2. The optical power in LN layer was 50.2%. For comparison, in a LNOI waveguide with a width of 1 μm and an etch depth of 250 nm, the optical mode area was 0.69 μm^2. Figure 2(c) shows the relationship between the bending loss and the bending radius. Compared with the LNOI waveguide, the Si loading strip waveguide allowed a smaller bending radius. When the bending loss was 10^{-6} dB/cm, the Si loading strip waveguide had a bending radius of approximately 30 μm, while the LNOI waveguide had a bending radius of approximately 70 μm. Here, the 90° circular bends had a radius of 50 μm. The TE optical mode was transmitted in the waveguide. The length difference of the asymmetric arms was $2\Delta L$. Due to the thin thickness of the Si thin film, part of the light of the waveguide resided in the LN layer. By applying a voltage to the metal electrodes, the refractive index of LN was changed and the interleaver could achieve the E-O tuning function. The E-O interaction length (L) was designed to be 1 mm, which was parallel to the Y axis of LN to take advantage of the large E-O coefficient r_{33} (28.6 pm/V at 1550 nm [15]) of LN. For efficient E-O tuning, the gap of metal electrodes was designed to be 2.6 μm, where the metal absorption loss was approximately 0.1 dB/cm for 800 nm wide Si loading strip waveguides.

A group of equally spaced wavelengths (λ_1, λ_2, λ_3, λ_4, ..., λ_{2n-1}, λ_{2n}) was input from the input port of the 1×2 MMI and then evenly distributed across the two asymmetric arms. After passing through the asymmetric arms, the phase difference between the two beams was: $\Delta\varphi_i = 4\pi\Delta L n_{eff}/\lambda_i$, where λ_i was the wavelength of the light, and n_{eff} was the effective refractive index of the waveguide. By carefully designing ΔL, light with wavelengths λ_1, λ_3, ..., λ_{2n-1}

Optics EXPRESS

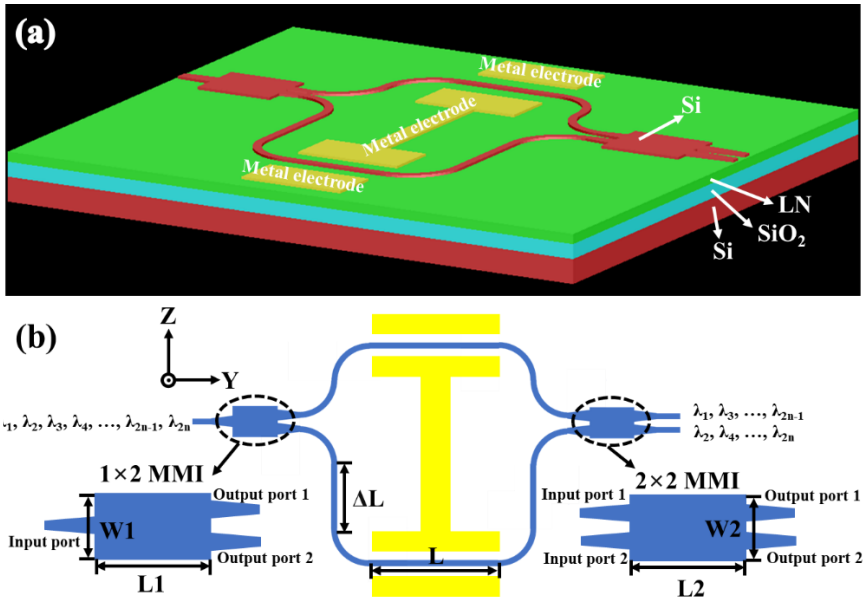

Fig. 1. (a) Schematic and (b) top view of the E-O tunable interleaver in Si-LNOI.

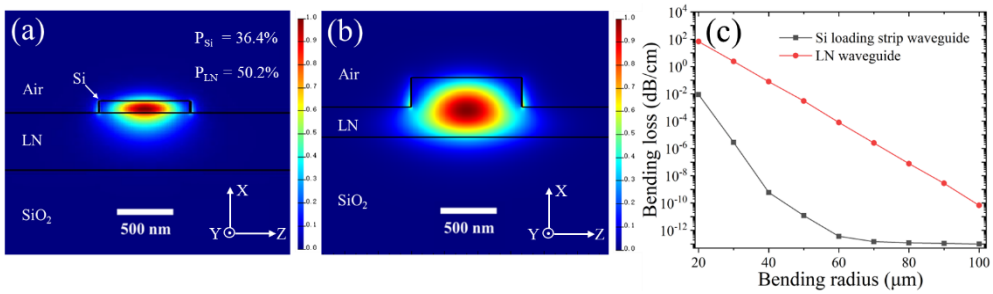

Fig. 2. Simulated optical TE modes of the (a) Si loading strip waveguide and (b) LNOI waveguide. (c) Relationship of waveguide bending loss with bending radius.

was constructive interference at output port 1 of the 2×2 MMI and destructive interference at output port 2 of the 2×2 MMI. However, light with wavelengths $\lambda_2, \lambda_4, \ldots, \lambda_{2n}$ was destructive interference at output port 1 of the 2×2 MMI and constructive interference at output port 2 of the 2×2 MMI. Therefore, the interleaver divided a group of densely spaced wavelengths into two groups of wavelengths that were sparsely spaced and interleaved with each other. Conversely, $\lambda_1, \lambda_3, \ldots, \lambda_{2n-1}$ and $\lambda_2, \lambda_4, \ldots, \lambda_{2n}$ were input from the two output ports of the 2×2 MMI, and light with wavelengths $\lambda_1, \lambda_2, \lambda_3, \lambda_4, \ldots, \lambda_{2n-1}, \lambda_{2n}$ could be output from the input port of the 1×2 MMI. Therefore, the interleaver could also converge two groups of wavelengths that were sparsely spaced and interleaved with each other into a group of densely spaced wavelengths. The working principle of the interleaver could also be described by the transmission matrix method. The transmission matrix of the interleaver is expressed as [16]:

$$[T] = \frac{1}{2}\begin{bmatrix} 1 & -j \\ -j & 1 \end{bmatrix}\begin{bmatrix} e^{-jL_a\beta_a} & 0 \\ 0 & e^{-jL_b\beta_b} \end{bmatrix}\begin{bmatrix} 1 \\ 1 \end{bmatrix} \tag{1}$$

Optics EXPRESS

where β_a and β_b are the propagation constants of the two asymmetric arms. L_a and L_b are the lengths of the two asymmetrical arms. When the light is input from the input port of the 1×2 MMI, the power values of the two output ports of the 2×2 MMI are expressed as [16]:

$$P_{\text{port 1}} = E^2 sin^2\left(\frac{\pi}{\lambda}\Delta L_{eff} + \frac{\pi}{4}\right) \tag{2}$$

$$P_{\text{port 2}} = E^2 \cos^2\left(\frac{\pi}{\lambda}\Delta L_{eff} + \frac{\pi}{4}\right) \tag{3}$$

where E is the amplitude of the input light, and λ is the wavelength. ΔL_{eff} is expressed as:

$$\Delta L_{eff} = \mathrm{n_{eff}} 2\Delta L \tag{4}$$

The channel spacing was one of the key parameters of interleaver, which was determined by ΔL. Due to the large $\mathrm{n_{eff}}$ (2.22) of the Si loading strip waveguide, the interleaver had a small ΔL and a small device size. Here, we designed the interleaver with an ΔL of 480 μm and a channel spacing of 50 GHz. The ER was another key parameter of interleaver, which was determined by the splitting ratio of MMIs. When the splitting ratio of the two MMIs was 1:1 (3 dB MMI), the amplitude response of the interleaver could be optimal, resulting in a large ER. The schematic structure of the 1×2 and 2×2 MMIs is shown in Fig. 1(b). An MMI consists of three parts: the input port, the multimode waveguide, and the output port. The input and output ports of the MMI were tapered to improve the performance of the MMIs. The self-imaging effect (SIE) is the basic theory of MMI [17]. For the 1×2 MMI, the input port was positioned at the center of the multimode waveguide. The position of the first 2-fold self-imaging is expressed as [18]:

$$L_{MMI} = \frac{3L_\pi}{8} \tag{5}$$

$$L_\pi = \frac{\pi}{\beta_0 - \beta_1} \tag{6}$$

where β_0 and β_1 are the propagation constants of the two lowest order modes. For the 2×2 MMI, the two input ports were located at $\pm\frac{W}{6}$ from the center of the multimode waveguide. The position of the first 2-fold self-imaging is expressed as [18]:

$$L_{MMI} = \frac{L_\pi}{2} \tag{7}$$

The greater the width of the multimode waveguide, the more modes could be excited in the multimode waveguide, with clearer self-imaging points and lower IL; however, as the width increases, the length of the multimode waveguide will also increase. Hence, there was a trade-off between IL and device size. We chose the width of the multimode waveguide of the 1×2 and 2×2 MMIs to be 3 and 6 μm, respectively. For the 1×2 MMI, the lengths of the input and output ports were 5 μm each, and their widths transitioned from 0.8 μm to 1.2 μm. Figure 3(a) shows the relationship between the transmission of the 1×2 MMI and the length (L1) of the multimode waveguide, which was simulated by the finite-difference time-domain method using FDTD within the aforementioned simulator. When L1 was 7.3 μm, the 1×2 MMI had the maximum transmittance of 98.74% (IL was 0.055 dB). The inset of Fig. 3(a) shows the field propagation of the optimized 1×2 MMI at the interface of the Si thin film and the LN thin film. Figure 3(b) shows the relationship between the transmission of the 1×2 MMI and the operating wavelength (when L1 was 7.3 μm). Because the short wavelength could excite more modes in the multimode waveguide to form clearer self-imaging points, the transmittance of the 1×2 MMI increased with the decrease of wavelength. For the 2×2 MMI, the lengths of the input and output ports were 10 μm each, and their widths transitioned from 0.8 μm to 1.4 μm. Figure 3(c)

Optics EXPRESS

shows the relationship between the transmission of the 2×2 MMI and the length (L2) of the multimode waveguide. When L2 was 36.4 μm, the 2×2 MMI had the maximum transmittance of 97.34% (IL was 0.117 dB). The transmittances of the two output ports of the 2×2 MMI were slightly different. A larger W2 could reduce the difference in transmittance between the two output ports, but it required a larger L2. The inset of Fig. 3(c) shows the field propagation of the optimized 2×2 MMI at the interface of the Si thin film and the LN thin film. Figure 3(d) shows the relationship between the transmission of the 2×2 MMI and the operating wavelength (when L2 is 36.4 μm). The transmittance of the 2×2 MMI decreased as the wavelength deviated from 1550 nm because the MMI length deviated from the self-imaging length. Compared with the 2×2 MMI, the 1×2 MMI had a larger operating wavelength range.

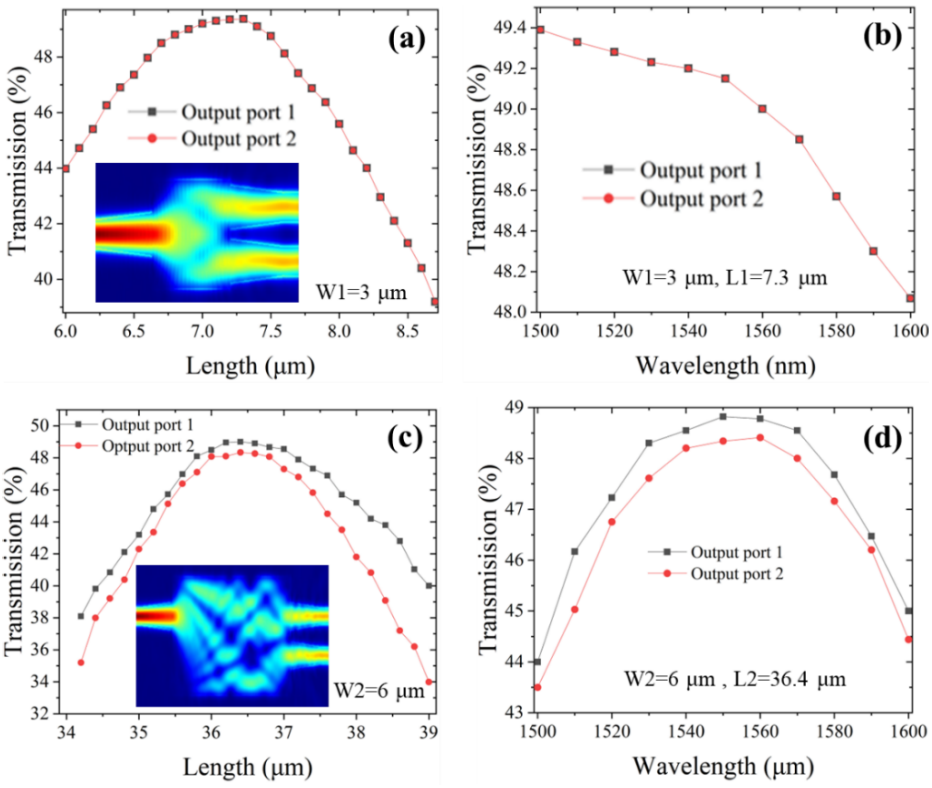

Fig. 3. Simulated transmission of the 1×2 MMI for different (a) multimode waveguide lengths (L1) and (b) operating wavelengths. Simulated transmission of the 2×2 MMI for different (c) multimode waveguides lengths (L2) and (d) operating wavelengths.

3. Experiments and discussion

The Si-LNOI was fabricated by bonding Si thin film on LNOI. The thickness of the Si thin film was 100 nm. The fabrication process of the E-O tunable interleaver is shown in Fig. 4. First, a layer of photoresist (HSQ) was spin-coated on the surface of the Si-LNOI sample. Then, the interleaver was patterned using electron beam lithography (EBL) and inductively coupled plasma (ICP) etching technology. Subsequently, a layer of photoresist (ZEP) was spin-coated on the surface of the sample and patterned using electron beam lithography (EBL). Next, metal electrodes were shaped using a lift-off process to achieve the E-O tuning function. Finally, the sample was cleaned using butanone to remove the residual photoresist and end-polished for

Optics EXPRESS

optical measurement. The length of the sample was 3.8 mm. An optical microscopy image of the fabricated E-O tunable interleaver is shown in Fig. 5(a). The values of L and ΔL were 1 mm and 480 μm, respectively. Figure 5(b) and (d) show the scanning electron microscope (SEM) images of the 1×2 and 2×2 MMIs, respectively. Figure 5(c) shows the SEM image of the metal electrodes and Si loading strip waveguide. The gap of electrodes was 2.65 μm. The width of the Si loading strip waveguide was 780 nm. The measured transmission loss of a straight Si loading strip waveguide was 9.8 dB/cm using the Fabry-Pérot method [19]. The transmission loss might be due to the scattering caused by the roughness of the side wall of the waveguide, and the scattering and absorption at the interface of LN thin film and Si thin film.

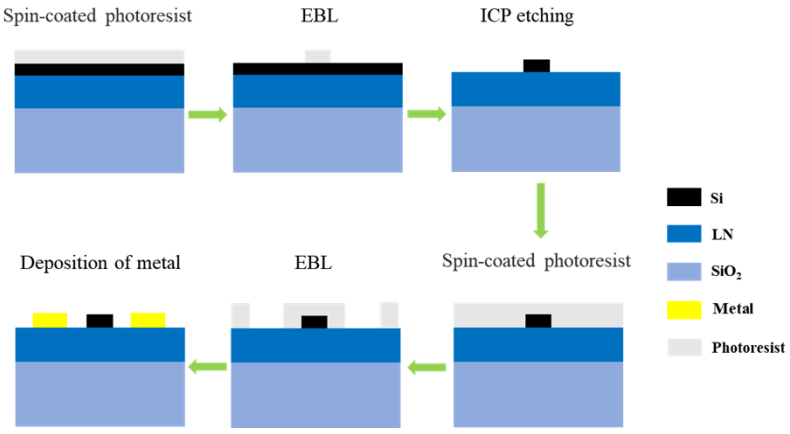

Fig. 4. Fabrication process of the E-O tunable interleaver in Si-LNOI.

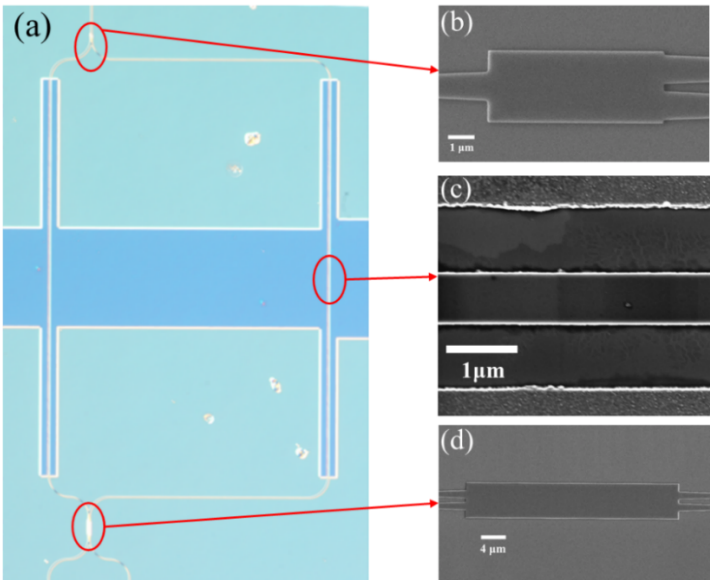

Fig. 5. (a) Optical microscopy image of the E-O tunable interleaver in Si-LNOI. SEM images of (b) the 1×2 MMI, (c) the metal electrodes, and (d) the 2×2 MMI.

Figure 6 shows the measurement system of transmission spectra of the interleaver. A continuous linear polarized light was emitted from a semiconductor tunable laser (Santec TSL-210VF), and

Optics EXPRESS

coupled into the input port of the 1×2 MMI via a lensed fiber. The polarization of the output light of the lens fiber could be adjusted by the positioner. The light from the two output ports of the 2×2 MMI was collected by an objective (40×/0.65) and then detected by the detector (Ge photodiode) after passing through the polarizer, splitter, and iris diaphragms. Among them, the polarizer was used to filter the TM mode that may exist in the waveguide to ensure the measurement accuracy of the ER of the interleaver. The splitting ratio of the splitter was 1:1. The iris diaphragms were used to filter stray light. Two detectors were used to detect the optical power from output ports 1 and 2 of the 2×2 MMI, respectively.

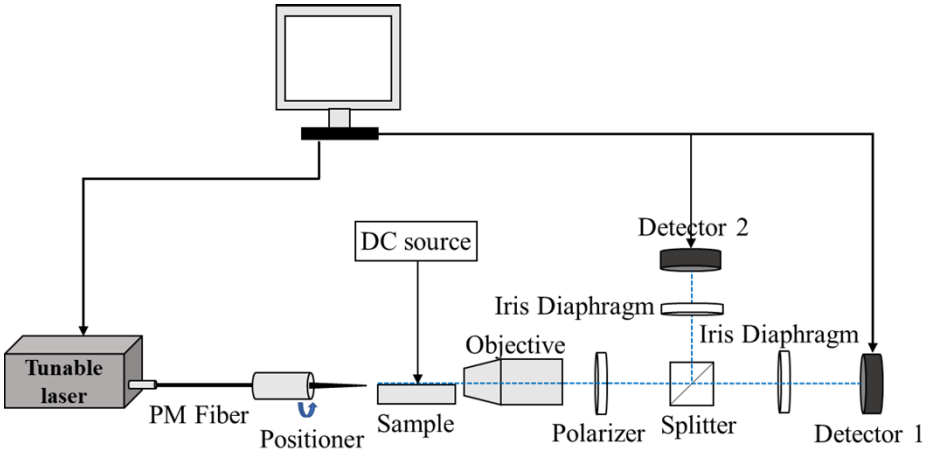

Fig. 6. Measurement system of transmission spectra of the interleaver.

Figure 7 shows the measured transmission spectra of the interleaver. As shown in Fig. 7(a), the interleaver had an ER of 12–28 dB and a channel spacing of 55 GHz in 1530–1620 nm. The channel spacing was larger than the designed channel spacing (50 GHz), which might be caused by the fabrication error of Si thin film and Si waveguide (making the n_{eff} of the Si loading strip waveguide smaller). The loss of the measurement system (including the objective, splitter and polarizer) was measured to be 6.5 dB. The IL of the interleaver was about 13.5 dB, which included the coupling loss between the waveguide and the lens fiber, the reflection at the end face of the waveguide, and the transmission loss of the Si loading strip waveguide. Among them, the measured coupling loss between the waveguide and the lens fiber was 7.8 dB/facet, and the simulated reflectance at the end face of the waveguide was 19%. In order to reduce the coupling loss between the waveguide and the lens fiber, the input and output waveguides of the interleaver could be designed to be tapered. In addition, the coupling loss could be further reduced by making spot-size converters [13] at input and output waveguides. To inspect the transmission spectra more clearly, the measured transmission spectra of the interleaver in 1545–1555 nm is shown in Fig. 7(b). The ripples of the transmission spectra might be caused by the interaction between the reflected light of the end face of the waveguide and the light in 2×2 MMI.

A voltage could be applied to the electrodes through a DC source, and the interleaver could realize the E-O tuning function. After applying −10 V, 0 V, and 10 V voltages to the electrodes, the transmission spectrum of the interleaver was recorded, and the results are presented in Fig. 8. The E-O modulation efficiency was 26 pm/V for an E-O interaction length of 1 mm, which could solve the problem of working wavelength drift caused by the fabrication error and environmental changes. The DC bias drift was observed in our fabricated interleaver, which was thought to be caused by the flow and redistribution of electrical charge in the LN region under DC voltage [20]. It was related to the internal defects of LN and the preparation process of the devices. The DC bias drift might be reduced by using the thermo-optical phase shifter [20]. The response

Optics EXPRESS

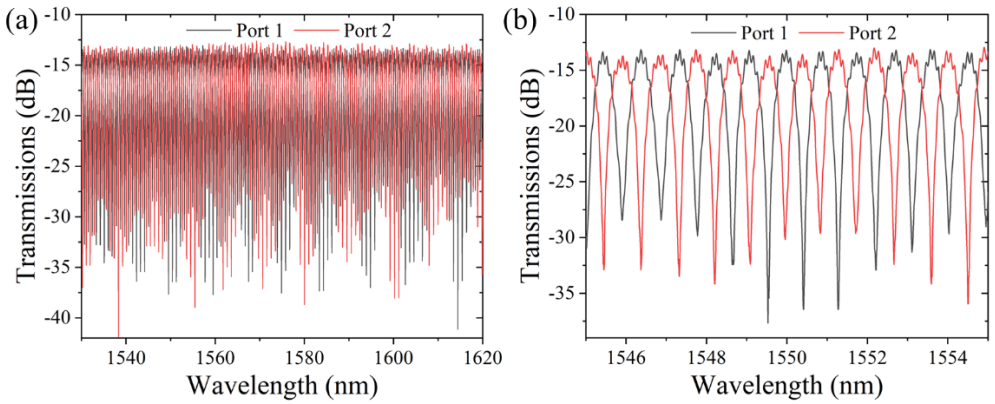

Fig. 7. Transmission spectra from output ports 1 and 2 of the 2 × 2 MMI in the range (a) 1530–1620 nm and (b) 1545–1555 nm.

speed of the interleaver was measured to be more than 1 MHz. If such a design was applied to the M-Z modulator, the $V_\pi L$ was only 1.7 V·cm, which was close to the state-of-the-art $V_\pi L$ of M-Z modulator in LNOI [21–23]. In addition, the device could be used as a tunable filter or a wavelength selective switch. For wavelength selective switches, a voltage of 17 V could achieve the on and off function. If the length of the E-O interaction region was lengthened appropriately, the interleaver could have higher E-O modulation efficiency. Table 1 shows a comparison of E-O tunable interleavers in different material platforms. The interleaver in Si-LNOI had a relatively high E-O modulation efficiency.

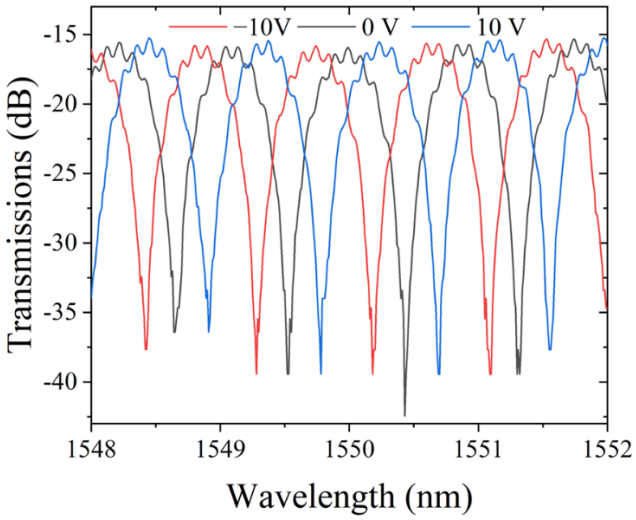

Fig. 8. E-O tunable characteristics of the interleaver.

Optics EXPRESS

Table 1. Comparison of E-O tunable interleavers in different material platforms.

Platform	ΔL (μm)	L (mm)	Channel spacing (GHz)	ER	E-O/T-O modulation
SOI [4]	225	–	50	18 dB	T-O (switching power of 50 mW)
LNOI [8]	707	1.35	49.7	10–20 dB for TE, 12–23 dB for TM	E-O (18 pm/V for TE, 16 pm/V for TM)
Si-LNOI (This work)	480	1	55	12–28 dB for TE	E-O (26 pm/V for TE)

4. Conclusions

In conclusion, we designed and fabricated an interleaver with an AMZI structure in Si-LNOI. The interleaver was fabricated by mature processing technology of Si photonic, and it was capable of the E-O tuning function by using the E-O effect of LN crystal. Due to the large n_{eff} and small mode area of the Si loading strip waveguide, the interleaver had a small arm length to reduce device volume and a small electrode gap to enhance E-O modulation efficiency. At 1530–1620 nm, the interleaver with ΔL of 480 μm achieved a channel spacing of 55 GHz and an ER of 12–28 dB. For an E-O interaction length of 1 mm, the E-O modulation efficiency was 26 pm/V. The interleaver will have potential applications in DWDM systems, optical switches, and filters.

Funding. National Key Research and Development Program of China (2018YFB2201700, 2019YFA0705000); Natural Science Foundation of Shandong Province (ZR2020LLZ007).

Disclosures. Houbin Zhu and Hui Hu are involved in developing lithium niobate technologies at Jinan Jingzheng Electronics Co., Ltd. (NanoLN). The other authors declare no conflicts of interest.

Data availability. Data underlying the results presented in this paper are not publicly available at this time but may be obtained from the authors upon reasonable request.

References

1. S. Cao, J. Chen, J. N. Damask, C. R. Doerr, L. Guiziou, G. Harvey, Y. Hibino, H. Li, S. Suzuki, K. Y. Wu, and P. Xie, "Interleaver technology: Comparisons and applications requirements," J. Lightwave Technol. **22**(1), 281–289 (2004).
2. W. Y. Chan, K. X. Chen, H. P. Chan, B. P. Pal, and R. K. Varshney, "A flattop PLC polymer waveguide interleaver based on folded two-stage-cascaded Y-junction Mach-Zehnder interferometers," Opt. Commun. **282**(5), 883–886 (2009).
3. J. F. Song, H. Zhao, Q. Fang, S. H. Tao, T. Y. Liow, M. B. Yu, G. Q. Lo, and D. L. Kwong, "Effective thermo-optical enhanced cross-ring resonator MZI interleavers on SOI," Opt. Express **16**(26), 21476–21482 (2008).
4. Z. G. Wu, S. Honda, J. Matsui, K. Utaka, T. Edura, M. Tokuda, K. Tsutsui, and Y. Wada, "Tunable monolithic DWDM band-selection interleaver filter switch on silicon-on-insulator substrate," J. Lightwave Technol. **26**(19), 3363–3368 (2008).
5. Y. F. Qi and Y. Li, "Integrated lithium niobate photonics," Nanophotonics **9**(6), 1287–1320 (2020).
6. J. T. Lin, F. Bo, Y. Cheng, and J. J. Xu, "Advances in on-chip photonic devices based on lithium niobate on insulator," Photonics Res. **8**(12), 1910–1936 (2020).
7. D. Zhu, L. B. Shao, M. J. Yu, R. Cheng, B. Desiatov, C. J. Xin, Y. W. Hu, J. Holzgrafe, S. Ghosh, A. Shams-Ansari, E. Puma, N. Sinclair, C. Reimer, M. Zhang, and M. Lončar, "Integrated photonics on thin-film lithium niobate," Adv. Opt. Photonics **13**(2), 242–352 (2021).
8. X. P. Li, K. X. Chen, and L. F. Wang, "Compact and electro-optic tunable interleaver in lithium niobate thin film," Opt. Lett. **43**(15), 3610–3613 (2018).
9. X. P. Li, M. K. Wang, J. H. Li, and K. X. Chen, "Monolithic 1×4 reconfigurable electro-optic tunable interleaver in lithium niobate thin film," IEEE Photonics Technol. Lett. **31**(20), 1611–1614 (2019).
10. H. B. Zhu, Q. Y. Li, H. P. Han, Z. Y. Li, X. Q. Zhang, H. H. Zhang, and H. Hu, "Hybrid mono-crystalline silicon and lithium niobate thin films," Chin. Opt. Lett. **19**(6), 060017 (2021).
11. Q. Y. Li, H. B. Zhu, H. H. Zhang, and H. Hu, "Phase modulators in hybrid silicon and lithium niobate thin films," Opt. Mater. Express **12**(4), 1314–1322 (2022).
12. J. Wang, S. F. Xu, J. P. Chen, and W. W. Zou, "A heterogeneous silicon on lithium niobate modulator for ultra-compact and high-performance photonic integrated circuits," IEEE Photonics J. **13**(1), 1–12 (2021).
13. Q. Y. Li, H. H. Zhang, H. B. Zhu, Z. H. Chen, and H. Hu, "Edge coupling for hybrid mono-crystalline silicon and lithium niobate thin films," Opt. Mater. Express **12**(10), 4147–4154 (2022).

Optics EXPRESS

14. B. Fang, S. L. Gao, Z. Z. Wang, S. N. Zhu, and T. Li, "Efficient second harmonic generation in silicon covered lithium niobate waveguides," Chin. Opt. Lett. **19**(6), 060004 (2021).
15. K. Yonekura, L. H. Jin, and K. Takizawa, "Measurement of dispersion of effective electro-optic coefficients and of non-doped congruent $LiNbO_3$ crystal," J. Appl. Phys. **47**(7), 5503–5508 (2008).
16. X. P. Li, "Research on thin-film lithium niobate waveguides and photonic devices," Ph.D. thesis, University of Electronic Science and Technology of China, 2020, p. 49.
17. R. Ulrich and G. Ankele, "Self-imaging in homogeneous planar optical waveguides," Appl. Phys. Lett. **27**(6), 337–339 (1975).
18. L. B. Soldano and E. C. M. Pennings, "Optical multi-mode interference devices based on self-imaging: principles and applications," J. Lightwave Technol. **13**(4), 615–627 (1995).
19. Y. W. Wang, Z. H. Chen, L. T. Cai, Y. P. Jiang, H. B. Zhu, and H. Hu, "Amorphous silicon-lithium niobate thin film strip-loaded waveguides," Opt. Mater. Express **7**(11), 4018–4028 (2017).
20. S. H. Sun, M. B. He, M. Y. Xu, S. Q. Gao, Z. Y. Chen, X. Zhang, Z. L. Ruan, X. Wu, L. D. Zhou, L. Liu, S. Y. Yu, and X. L. Cai, "Bias-drift-free Mach–Zehnder modulators based on a heterogeneous silicon and lithium niobate platform," Photonics Res. **8**(12), 1958–1963 (2020).
21. Y. Liu, H. Li, J. Liu, S. Tan, Q. Y. Lu, and W. H. Guo, "Low V_π thin-film lithium niobate modulator fabricated with photolithography," Opt. Express **29**(5), 6320–6329 (2021).
22. P. Kharel, C. Reimer, K. Luke, L. Y. He, and M. Zhang, "Breaking voltage–bandwidth limits in integrated lithium niobate modulators using micro-structured electrodes," Optica **8**(3), 357–363 (2021).
23. X. C. Liu, B. Xiong, C. Z. Sun, J. Wang, Z. B. Hao, L. Wang, Y. J. Han, H. T. Li, J. D. Yu, and Y. Luo, "Wideband thin-film lithium niobate modulator with low half-wave-voltage length product," Chin. Opt. Lett. **19**(6), 060016 (2021).